REPRINT

SPIE—The International Society for Optical Engineering

Reprinted from

Proceedings of

Lasers in Surgery: Advanced Characterization, Therapeutics, and Systems VI

27–30 January 1996
San Jose, California

Volume 2671

Computational modeling of laser thrombolysis for stroke treatment

Moshe Strauss
University of California Davis, Department of Applied Science, Livermore, California 94550, and the Nuclear Research Center, Negev, P.O. Box 9001, Beer Sheva, Israel.

Peter Amendt, Richard A. London, Duncan J. Maitland, Michael E. Glinsky, Peter Celliers, David S. Bailey, and David A. Young
Lawrence Livermore National Laboratory, Livermore, California 94550

Steven L. Jacques
University of Texas-M.D. Anderson Cancer Center Houston, Texas 77030

ABSTRACT

Many aspects of the physical processes involved in a pulsed laser interacting with an occlusion in the intra-cranial vascular system, e.g., a blood clot, are included in the simulation codes LATIS and LATIS3D. Laser light propagation and thermo-mechanical effects on the occlusion can be calculated by these codes. The hydrodynamic response uses a realistic equation of state which includes melting and evaporation. Simple material strength and failure models now included in these codes are required to describe clot breakup. The goal is to ascertain the feasibility of laser thrombolysis, and to help optimize the laser parameters for such therapy. In this paper detailed numerical results for laser interaction with water is considered as an initial model for laser thrombolysis of soft blood clots which have high water content. Three regimes of water response to increasing laser energy are considered: (1) the linear stress pulse, (2) the nonlinear evaporation bubble, and (3) the nonlinear inertial bubble. It is shown that later in time the inertial bubble evolves into a slowly growing cavitation bubble. More physical processes will be added in the near future to better model realistic occlusion-vessel wall geometries.

Keywords: Laser thrombolysis, stress waves, evaporation bubble, cavitation, equation of state, failure models.

2. INTRODUCTION

Laser thrombolysis has been extensively studied in the field of interventional cardiology.[1] Recently it has been proposed to use laser thrombolysis to assist treatment of stroke. The laser light is destructively coupled to an occlusion that obstructs the blood flow in intracranial arteries. This occlusion is generally a type of blood clot but can also consist of plaque. Our goal is to optimize laser parameters for such therapy. For this purpose a computer code is being developed that models the important physical processes for laser thrombolysis.

The goal of the computational effort is based on constructing two-dimensional (2D) simulations which include the following physics: laser coupling to the clot, hydrodynamics including elasticity, realistic equations of state (EOS) for the materials involved, models for material failure and damage, and integrity of the vessel wall.

Soft tissues such as blood clots have high water content and can be approximated by a water EOS. We study a simplified laser-water system in order to identify the various coupling regimes. We identify three different regimes of

operation. The linear regime for low laser energies is characterized by stress waves which are emitted from the heated region with temperatures remaining below the boiling point. The non-linear evaporation bubble regime occurs for higher laser energy, where the heated region obeys $100\ ^{0}C < T < 400\ ^{0}C$. Further increase of the laser energy induces a fast bubble expansion. We call this stage an inertial bubble regime due to the induced motion of matter surrounding the bubble. Later in time this bubble evolves into a slowly growing cavitational bubble.

The laser-water interaction study can be a useful initial model towards considering lysis of soft blood clots. However, calculations including more realistic physics should be considered as discussed in the following sections.

The paper is organized as follows: §3 discusses the physical elements of the problem and the computer code required to model laser thrombolysis, §4 analyzes the various regimes in laser-water interaction, and concluding remarks are presented in §5.

3. COMPUTATIONAL MODEL OF LASER THROMBOLYSIS

Computational modeling of laser thrombolysis involves nonlinear coupling of a variety of physical processes. Most of them are contained in a computer code developed at LLNL called LATIS (LAser TISsue).[2] This code can be used as a predictive design tool for laser thrombolysis. The physical processes involved can be grouped in four areas as shown in fig. (1). Laser propagation through the occlusion involves various absorption and scattering processes which can be included using a Monte-Carlo treatment. A simplifying assumption is to apply an exponential deposition of laser energy in space based on Beer's Law. The hydrodynamic response involves the conservation equations for the local mass, momentum and energy and depends on the EOS for a determination of the main thermodynamic quantities: pressure, temperature and entropy. For realistic tissue such as a blood clot, it is important to extend the hydrodynamics to include the elasticity of the medium. This extension for including shear forces replaces the scalar pressure by a 3×3 matrix that couples the motion in various directions and affects local energy balance.

The thermal response is based on a heat diffusion equation and includes various cooling and heating processes. In general the thermal response of soft tissue operates on a longer time scale relative to the hydrodynamics and can be ignored on a hydrodynamic time scale. In soft tissue with high water concentration, the thermal response time scale is on the order of a millisecond for a laser deposition region of the order of 10 μm. For a typical system dimension of several millimeters and with a water sound velocity of about 1500 m/sec, the hydrodynamic time scale is much less than a millisecond.

The material response is incorporated by using a realistic EOS. The EOS tables for an extended class of tissue can be constructed with reasonable accuracy by using the quotidian equation of state method (QEOS).[3] This method is based on a phenomenological treatment using the measured macroscopic properties of the tissue such as melting and boiling temperature, vapor pressure, bulk modulus, thermal expansion coefficient and cohesive energy. Increasing the number of measured variables improves the accuracy of the EOS. The method ignores molecular structure and can be applied towards a variety of tissues and materials involved in laser thrombolysis. In addition, the code has access to the Los Alamos National Laboratory SESAME EOS tables for a wide assortment of materials.[4] A very detailed QEOS table for biological materials and water is still under development. Thus for the computational results in the next section we use the SESAME EOS for water.

To promote the breakup of occlusions we need to apply a stress-strain model together with an appropriate failure model. Most tissue response obeys a linear (Hooke's Law) behavior for low stress, but deviates at high stress in a variety of ways.[5] It is important to identify the nature of the stress-strain relation for the material at hand in order to understand possible failure mechanisms. Most soft tissue fails easily under tensile and shear stresses relative to compressional stresses. For a soft blood clot to fail under tensile or shear stress requires a stress of order 10-50 bar.[6] Our code has the capability to choose among several simple macroscopic failure models. More detailed models are based on statistical mechanical methods. For example, a failure which generates voids or cavitational bubbles can be represented in terms of a statistical mechanics ensemble of elements of various dimensions.[7] These models will be considered in the future.

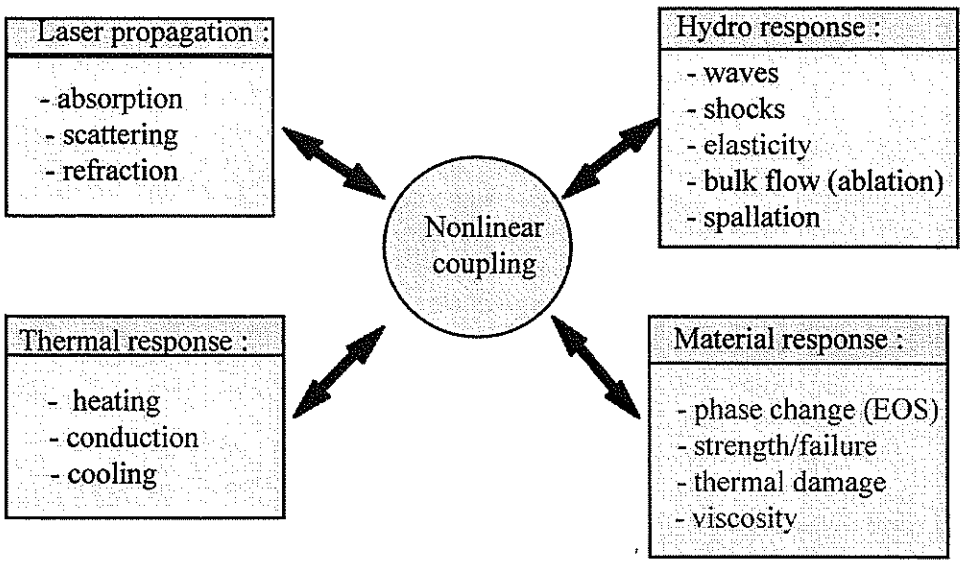

Fig. 1. The physical processes involved in laser thrombolysis are grouped into four areas: laser propagation, hydro response, thermal response and material response.

Most soft tissue consists of composite materials. For example, blood clots contain blood cells (platelets and red blood cells) fastened together by protein-based fibrin fibers. The blood cells consist mainly of water. Thus, an approximate EOS for blood clots can be based on a water EOS and under negative pressure (or tension) its failure is limited by the fibrin fibers.

The water EOS is of special importance for many tissues of high water content. In fig. (2) we use a high resolution QEOS table for water to show the pressure P as a function of the specific volume $V=1/\rho$ along various isotherms (constant temperature) and adiabats (constant entropy). Near normal density ($\rho=1$ g/cm^3) the system is almost incompressible so that a small change in volume requires a large change in pressure. Some processes lead towards negative pressure (tension). Although the tensile strength of pure water is in the several 100 bar range, in most cases the presence of impurities reduces it to the range of 10 bar. For intermediate temperatures, $T < T_c$, where T_c is the critical temperature for single phase existence, water can be in a coexisting mixed state of liquid-vapor. In water T_c=374 ^{0}C and the related critical pressure is P_c=218 bar.[8] For temperatures $T > T_c$, there is a smooth transition from liquid to vapor state and the system behaves close to an ideal gas. In many practical cases as considered in the next section, the hydrodynamic response is faster than thermal relaxation. Locally, the change in energy is not from thermal diffusion but from internal specific energy and from the work done on the volume element of interest by its surroundings. In this case the entropy is constant in the process and the system follows an adiabatic expansion as shown in fig. (2).

We have the capability to calculate the effect of cumulative thermal damage by applying an Arrhenius rate model which depends exponentially on the local temperature. This will be considered in future work to model possible thermal damage to the vessel walls.

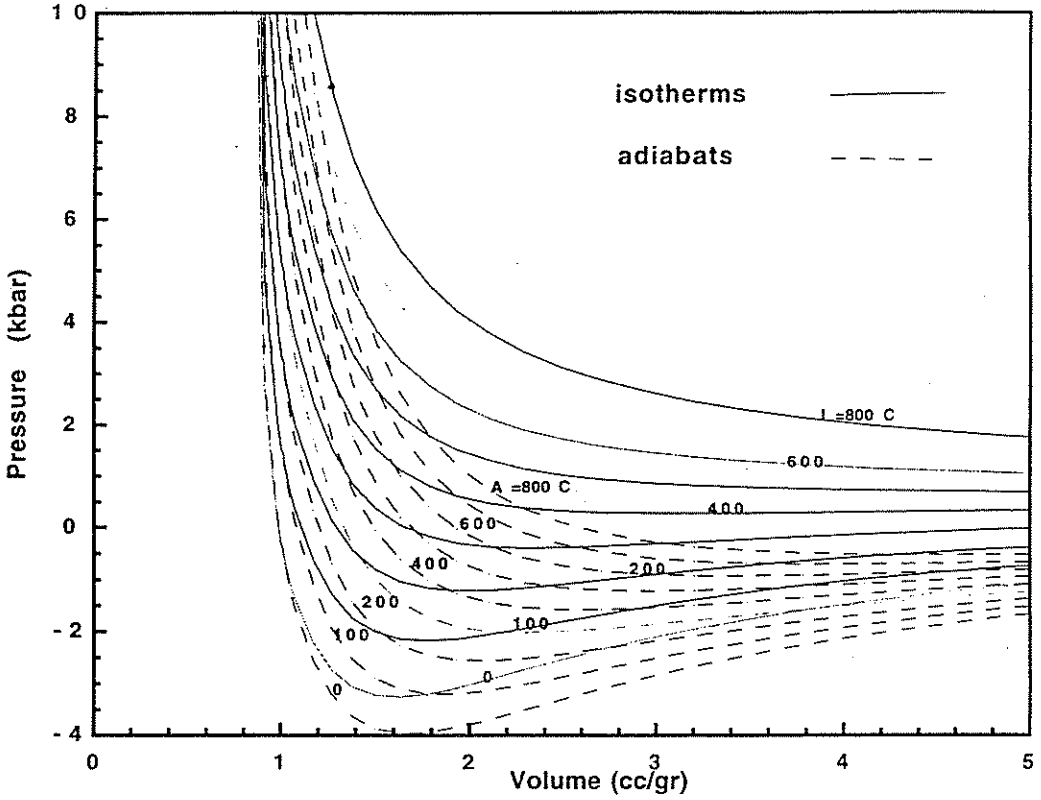

Fig. 2. Pressure vs specific volume $V=1/\rho$ for isotherms (solid lines for temperatures in the range 0-800 ^{0}C), and adiabats (dashed lines), where at V=1 cc/g the isotherms and adiabats are at the same temperatures.

Many soft tissues such as blood clots are viscous materials. It is important to include this property in the computational model. Viscosity can affect the hydrodynamic motion and the energy balance in the system by acting as a dissipative sink of energy. The hydrodynamic codes presented here ignore this effect; future work will consider this mechanism.

It is important that the computational effort evolve to consider two-dimensional effects. Two computer codes have been developed with most of the physics presented in fig.(1). The first code is LATIS and is a two dimensional code based on mainly finite difference techniques. The basis for this code is the code LASNEX which has been test for over twenty years on a variety of physical problems in a multi-user environment. [9] The second code is LATIS3D which is a three-dimensional code based on finite elements. This code is new and is based on the code ICF3D. [10] The code LATIS3D will be available in the future for collaboration. In the following, the aforementioned codes are used to investigate the coupling between laser light and a blood clot using the water EOS as a first approximation.

4. COMPUTATIONAL RESULTS FOR LASER-WATER INTERACTION

To study the various regimes of laser-soft tissue interaction, as in a blood clot, we consider a system of water interacting with a laser of varying energy. We consider here a wide optical fiber embedded in water so that the guided laser-tissue interaction can be well approximated by a one-dimensional planar geometry. The light absorption is modeled via Beer's Law which generates exponential deposition profiles. We assume a short pulse of laser in the nanosecond range. Thus, laser deposition can be considered as an essentially instantaneous process.

Initially the water is assumed to be at an ambient temperature T_0 =17 ^{0}C with an absorption coefficient of μ_a =1000 cm^{-1}. A SESAME EOS for water is used. A reflection boundary condition of the water response is assumed at the fiber boundary. Three regimes of response are identified depending on the laser energy. For low laser energy which heats the water to an initial temperature below boiling (T< 100 ^{0}C), linear stress pulse propagation is obtained. For intermediate laser energy (100 ^{0}C <T<400 ^{0}C), a nonlinear regime characterized by the formation of an evaporation bubble is obtained. Further increasing the laser energy to obtain yet higher water temperatures (T>400 ^{0}C) generates an evaporation bubble that evolves into a slowly growing cavitational bubble. We call this regime the inertial bubble regime. In the following we consider these three regimes of hydrodynamic response.

4.1. Linear stress wave regime

We start by considering a laser of energy fluence F=0.14 J/cm^2 propagating in the x direction and heating the water at position x=0 to temperature T=51 ^{0}C . In figs. (3a-3d) we present the pressure P, density ρ, fluid speed u and temperature T , respectively, as a function of position for time t=50, 100, 150, 200 nsec. Figure (3a) shows a stress pressure pulse that is launched from the heated region. The wave is symmetric in shape because of the reflecting boundary condition at the fiber surface. AS expected the maximum of the pressure pulse is about half of its initial value and reaches a value of about 140 bar. The wave moves to the right and is almost unaltered in shape. Figures (3b-3d) present the other variables: density, speed and temperature, which have a similar behavior to the pressure wave away from the heated region. We see that close to x=0 there is a heated region with reduced density which stays unchanged over hydrodynamic timescales.

The launched pulses for the various variables are similar in shape and are amenable to a linear approximation for the amplitudes. It is of interest to derive scaling law relations between the various physical maxima. We use a linear expansion for the variables: density $\rho = \rho_0 + \rho_1$, fluid speed $u = u_1$, pressure $P = P_0 + P_1$, and energy $e = e_0 + e_1$, where ρ_0=1 g/cm^3 and $\rho_1 << \rho_0$. Here, P_0 = 1 bar, $P_1 >> P_0$, and the sound speed c_s is much greater than u_1 . In the linear approximation, all terms higher than first order are ignored. We use the following hydrodynamic equations in planar geometry,

$$\frac{d\rho}{dt} + \rho \frac{\partial u}{\partial x} = 0 \qquad \text{(1a)}$$

$$\rho \frac{du}{dt} = -\frac{\partial P}{\partial x} \qquad \text{(1b)}$$

$$\rho \frac{de}{dt} = -P \frac{\partial u}{\partial x} \qquad \text{(1c)}$$

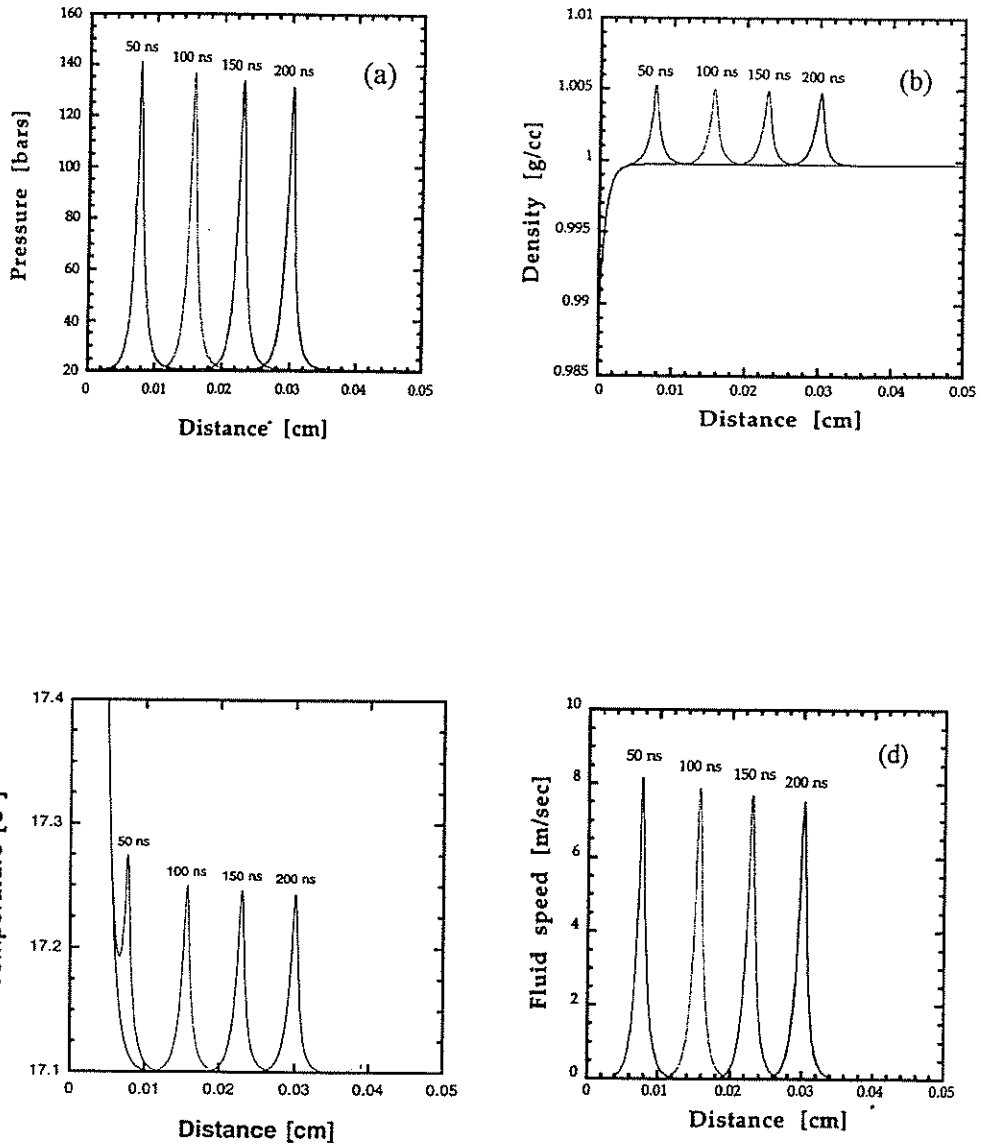

Fig. 3. Pressure (a), density (b), temperature (c) and fluid speed (d) vs distance for times 50, 100, 150, 200 nsec. The absorption coefficient is μ_a=1000 cm^{-1} and fluence F=0.14 J/cm^2.

where $\frac{d}{dt} = \frac{\partial}{\partial t} + c_s \frac{\partial}{\partial x}$. We assume a wave solution $f(\varsigma)$ for all of the physical variables, where $\varsigma = x - c_s t$. We write $P(\rho, T)$ and use the expansion,

$$\frac{\partial P}{\partial x} = \left(\frac{\partial P}{\partial \rho}\right)_T \cdot \frac{\partial \rho}{\partial x} + \left(\frac{\partial P}{\partial T}\right)_\rho \cdot \frac{\partial T}{\partial x} \tag{2}$$

where $\left(\frac{\partial P}{\partial \rho}\right)_T = 1/(\rho\, \kappa_T)$ is related to the isothermal compressibility κ_T, where $\kappa_T = 1/(\rho_0 c_s^2)$. For low compressibility the second term on the r.h.s. of eq. (2) can be ignored as seen from fig.(2) near volume 1 cm^3/g .

We further expand the specific local energy $e(\rho, T)$,

$$\frac{\partial e}{\partial x} = \left(\frac{\partial e}{\partial \rho}\right)_T \frac{\partial \rho}{\partial x} + \left(\frac{\partial e}{\partial T}\right)_\rho \frac{\partial T}{\partial x} \tag{3}$$

where $\left(\frac{\partial e}{\partial T}\right)_\rho = c_V$ is the heat capacity at constant volume, and $\left(\frac{\partial e}{\partial \rho}\right)_T = -P_e/\rho^2$ with P_e as the elastic pressure [11]. From eqs.(1a,1b) and the above approximations, a wave equation can be obtained for ρ_1, u_1, P_1 with the sound speed c_s . Using eqs.(1a,1b,1c) with above approximations, the following scaling law relations are obtained between the maxima of the various variables P_{IM}, ρ_{IM}, u_{IM}:

$$u_{IM} = \frac{P_{IM}}{\rho_0\, c_s} \tag{4a}$$

$$\rho_{IM} = \rho_0 \frac{u_{IM}}{c_s} \tag{4b}$$

$$T_{IM} = \frac{\left(u_{IM}^2 + \rho_{IM} \cdot P_e/\rho_0^2\right)}{c_V} \tag{4c}$$

In eq. (4a), u_{IM} is proportional to P_{IM} . For u_{IM} very small compared to c_s we get in eq. (4b) that ρ_{IM} is very small relative to ρ_0. The first term in eq. (4c) is the thermal energy contribution from the local $-P \cdot dV$ work. The second term in eq. (4c) is related to the effect of compression on the internal energy. The above scaling relations agree very well with our computational results. They can be useful in various application with realistic EOS tables.

4.2. Nonlinear evaporation bubble regime

The nonlinear regime is obtained for laser fluences that raise the initial temperature above the boiling point. For temperatures approximately in the range 100 ^{0}C < T < 400 ^{0}C, an evaporation bubble is generated which launches a nonlinear pulse from the heated region. We consider here a laser fluence of F=1.4 J/cm^2 that initially heats the water at x=0 to a temperature T = 356 ^{0}C . In figs. (4a) and (4b) we present the pressure and density, respectively, as a function of distance x for time t=50, 100, 150, 200 nsec. The nonlinear effect is to steepen the forward part of the launched pulse because of dispersion. We obtain a further decrease in height and an increase in width as the pulse propagates away from the heated region. The pulse shape is similar for the various hydrodynamic variables because of coupling. The density reduction in the heated region reaches a low density of 0.75 g/cm^3 on a hydrodynamic time scale. This value is consistent with the corresponding adiabat of fig. (2). We plan in the future to obtain the scaling law relations between the various variables in this nonlinear region in order to understand the coupling in detail.

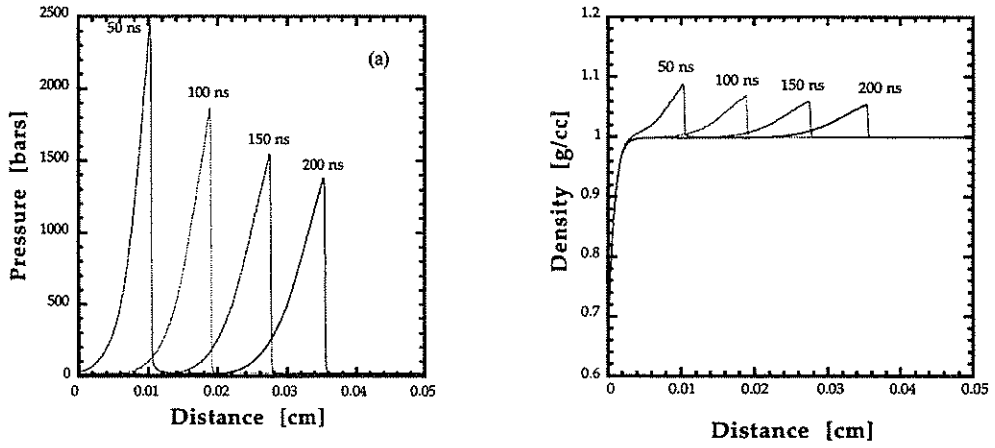

Fig. 4. Pressure (a) and density (b) vs distance for times 50, 100, 150, 200 nsec. The absorption coefficient μ_a=1000 cm^{-1} and fluence F=1.4 J/cm^2.

4.3. Nonlinear inertial bubble regime

Further increasing the laser energy to temperatures approximately above 400 ^{0}C produces even larger nonlinearity which affects strongly the evolution of the bubble region. As an example, we consider a laser fluence of F=5.6 J/cm^2 that raises the water temperature at x=0 to T= 1373 ^{0}C. The initial reduction of the density at x=0 is to 0.15 g/cm^3. Figures (5a) and (5b) show the pressure and fluid speed, respectively, as a function of distance x for time t=50, 100, 150, 200 nsec. From fig. (5a) the residual pressure near x=0 strongly affects the evolution of the bubble region. As a result, the mass surrounding the bubble is set to higher speed as can be seen in fig. (5b). Due to this inertia the bubble continues to expand. Later in time this inertial bubble evolves into a slowly growing cavitational bubble.

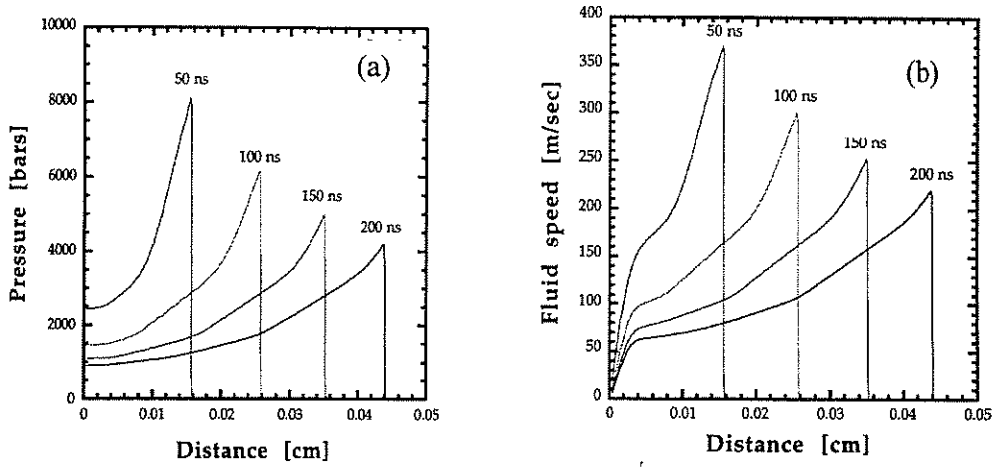

Fig. 5. Pressure (a) and fluid speed (b) vs distance for times 50, 100, 150, 200 nsec. The absorption coefficient μ_a=1000 cm^{-1} and fluence F=5.6 J/cm^2

In fig. (6a) we present the density as a function of distance for much longer times ranging from 1 to 150 μs for a fluence F=11.2 J/cm^2. A well-defined bubble with reduced density is obtained. The bubble size grows from 10 μm to 1000 μm in 150 μs. Figure (6b) shows the bubble size as a function of time for two values of laser fluence F=5.6 J/cm^2 and 11.2 J/cm^2. As the fluence is doubled, the size of the bubble is doubled on the same long timescale. Thus, we have obtained cavitational bubbles in planar geometry.

In the future we intend to also study spherical bubbles in various regimes. We expect to obtain spherical cavitation on a shorter time scale because of three dimensional effects acting to reduce the outgoing pressure pulse more effectively. We further intend to compare the spherical bubble with ongoing experiments.[12]

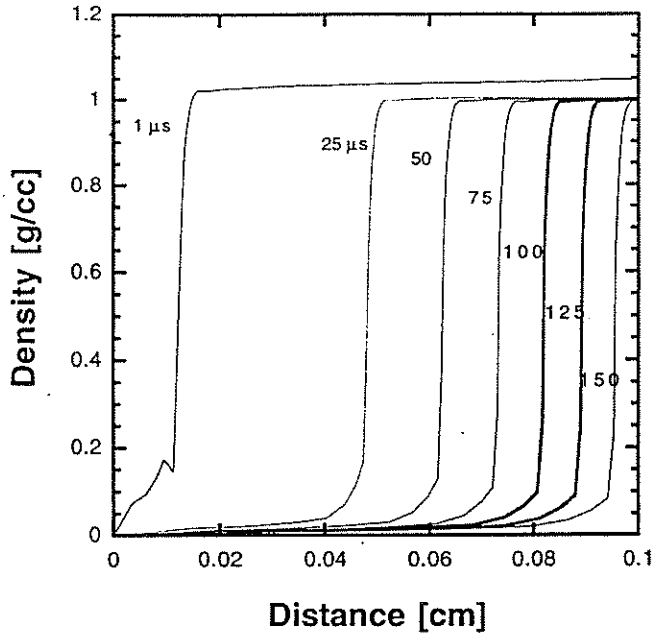

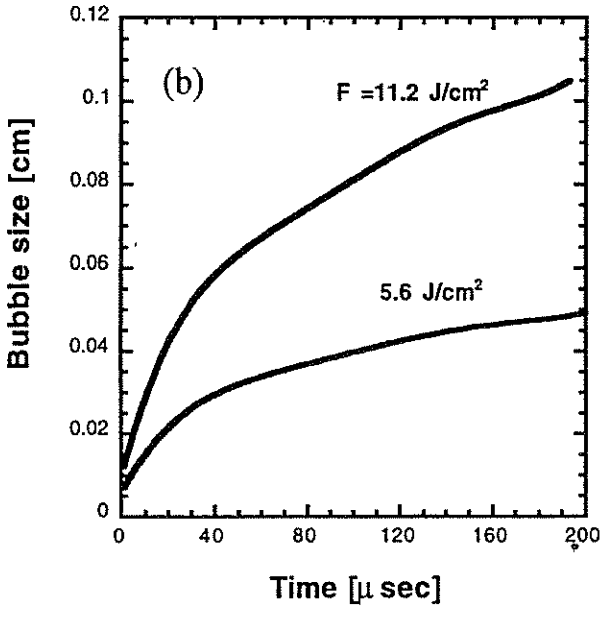

Fig. 6. (a) Density vs distance for times 1, 25, 50, 75, 100, 125, 150 μs and fluence F=11.2 J/cm^2. (b) The bubble size vs time for fluences F=5.6 J/cm^2 and 11.2 J/cm^2. The absorption coefficient is μ_a=1000 cm^{-1}.

5. CONCLUSIONS

The computer codes LATIS and LATIS3D incorporate most of the physical processes required to understand the conditions for laser thrombolysis. We have identified three regions of response of the water system to various values of laser energy which can be useful for laser-soft tissue coupling as in laser thrombolysis. The three regimes are: (1) the linear stress wave regime, (2) the nonlinear evaporation bubble regime and (3) the inertial bubble which evolves to a cavitation bubble. We intend to consider spherical bubbles in similar detail and to compare with experimental results.

For practical considerations, a variety of physical processes should be added systematically in considering laser thrombolysis: two-dimensional effects including the occlusion and the vessel wall, realistic EOS for the relevant materials, and failure models under tension and shear. Viscosity is not presently included in the codes, but its effect should be understood and quantified.

6. ACKNOWLEDGMENTS

We wish to thank Luiz Da Silva and Dennis Matthews for helpful discussions. We also thank R. Hermes of LANL for bringing to our attention several references on blood clot properties. This work was performed under the auspices of the DOE by the Lawrence Livermore National Laboratory under contract W-7409-ENG-48.

7. REFERENCES

1. K. Gregory, "Laser thrombolysis", In *Interventional Cardiology*, E. J. Topol, editor, **vol. 2**, ch. V, p. 892 (W. B. Saunders Company, 2 ed., 1994).
2. R. A. London, M. E. Glinsky, G. B. Zimmerman, D. C. Eder and S. L. Jacques, "Coupled light transport-heat diffusion model for laser dosimetry with dynamic optical properties", in *Laser Tissue Interaction VI*, S. L. Jacques, editor, Proc. SPIE **2391** (1995), p. 434.
   M. E. Glinsky, R. A. London, G. B. Zimmerman, and S. L. Jacques, "Modeling of endovascular patch welding using the computer program LATIS," in *Laser Tissue Interaction VI*, S. L. Jacques, editor, Proc. SPIE **2391** (1995), p. 262.
3. R. M. More, K. H. Warren, D. A. Young, and G. B. Zimmerman, "A new quotidian equation of state (QEOS) for hot dense matter", Phys. Fluids **31**, 3059 (1988).
   D. A. Young, and E. M. Corey, "A new global equation of state model for hot dense matter", J. Appl. Phys.,**78**, 3748 (1995).
4. K. S. Holian, editor, "T-1 handbook of material properties data bases, vol. Ic: equation of state", Los Almos: LA-10160-MS, UC-34, 1984.
   S. P. Lyon and J. D. Jonhson, editors, "Sesame: the Los Almos National Laboratory equation of state database", Los Almos: LA-UR-92-3407, (1992).
5. J. Vincent, *Structural Biomaterials* (Princeton University Press, New Jersey 1990).
   Y. C. Fung, *Biomechanics-motion flow stress and growth* (Springer-Verlag, New York 1990).
6. R. G. Macfarlane and A. H. Tomlinson, "Technical methods-An apparatus for measuring the tensile strength of blood clots", *J. Clin. Path.*, **14**, 320(1961). H. Hartert, and J. A. Schaeder, "The physical and biological constants of thrombelastography", *Biorheology*, 1 , 31 (1962).
   G. Paltauf and H. Schmidt-Kloiber, "Study of different ablation models by use of high-speed-sampling photography", in *Laser Tissue Interaction III*, S. L. Jacques, editor, Proc. SPIE **1646** (1992), p.343.
7. D. R. Curran, L. Seaman, and D. A. Shockey, "Dynamic Failure of Solids", Physic report, **147**, 253 (1987).
   T. Antoun, L. Seaman, D. Curran, and M. Glinsky, "Damage and failure Mechanisms associated with photoablation of biological tissues", To be published in *the Proceedings of the 1995 APS topical conference on shock compression of condensed matter*, Seattle, WA, edited by S. C. Schmidt et. al, AIP Press.
8. R. C. West, editor, *Handbook of chemistry and physics* (CRC Press, 56th ed.) p. F- 86 .
9. G. B. Zimmerman and W. L. Kruer, "Numerical simulation of laser initiated fusion", Commun. Plasma Phys. Controlled Fusion, **11**, 82 (1975).
10. D. S. Kershaw, M. K. Prasad, and M. J. Shaw, "3D unstructured mesh ALE hydrodynamics with the upwind discontinuous finite element method", LLNL report UCRL-JC-122104, to be published in J. of Computational Physics.
11. Ya. B. Zel'dovich, and Yu. P. Raizer, *Physics of shock waves and high- temperature hydrodynamic phenomena* (Academic press New York 1967) Volume II, p.690.
12. P. Celliers, L. B. Da Silva, N. J. Heredia, B. M. Mammini, R. A. London, D. L. Matthews and M. Strauss, " Dynamics of laser-induced transients produced by nano second laser pulses", *in Laser Tissue Interaction VII*, S. L. Jacques, Editor, Proc. SPIE **2671A** (1996), in this proceedings.